SECED 2023 Conference
Earthquake Engineering & Dynamics for a Sustainable Future
14-15 September 2023, Cambridge, UK

ANALYTICAL PARAMETRIC INVESTIGATION OF NONLINEAR TRAIN-STRUCTURE INTERACTION UNDER EARTHQUAKE EXCITATION

Miguel GOMEZ[1] & Matthew DEJONG[2]

Abstract: *Railway infrastructure plays an important role in countries' economies. The aging of such infrastructure and the lack of fast methods to quantify the operational resiliency of railroad systems under different hazards pose a concern to local governments that is to be addressed. Since train-structure interaction is a complicated phenomenon, involving many variables from the train, the structure, and the layer connecting both systems, past research has focused on how to precisely determine the response of a bridge-structure system under earthquake excitation. However, an analytical study that allows running simplified simulations, enabling faster evaluation of the response of a railway system at a regional scale is still to be done. In this study, an analytical model of a train-bridge system is presented and used to perform a parametric investigation on the performance of railway systems under earthquake excitation. A linear multibody model with springs and dashpots is used to simulate the train and its suspension system, a nonlinear frame model is used for the concrete bridge supporting structure, and the interface model, based on Kalker's linear theory, allows for rocking, sliding, and derailment of the train. The model provides predictions of the global response parameters of both the bridge and the train, allowing investigation of how the nonlinear bridge response affects derailment of the train and the main parameters that control the response of the system. The results show a good correlation between the peak bridge velocity and train derailment. Additionally, the results indicate that plastic behavior of the bridge column leads to a decreased likelihood of derailment of the train, despite the period lengthening that occurs.*

Introduction

Railway infrastructure plays an important role in the economic development of a country. In the United States, 140,000 miles of railway moves an industry of nearly 80 billion USD (Federal Railroad Administration, 2023). Thanks to its reliability, cost-effectiveness and low life-cycle carbon footprint, nations across the globe are strengthening their railway systems for both passenger and freight transportation. California High-Speed Rail, now under construction, is a clear example of such development. Notwithstanding this, multiple recent developments on high-speed trains and existing railway infrastructure in general are located in earthquake-prone regions. For example, most of China's high-speed railway network runs over bridges or elevated structures, with long portions in highly active seismic regions. In Japan, earthquakes have also caused train derailments, most of them while running on bridges. Just last year, the Tohoku Shinkansen train derailed after a M7.4 earthquake; while there were no casualties and all passengers and crew resulted unharmed, the derailment caused damage to the rails and equipment, and operation was suspended for several hours (The Japan Times, 2022).

The rapid development of railway networks, the aging of existing infrastructure in earthquake-prone regions, and the lack of methods for evaluating their resilience under natural hazards including earthquakes and strong winds have led to an increased interest in the development of procedures and methods for the analysis of trains running over bridges and elevated structures, accounting for as many elements as possible during the simulation. Lately, many research groups has focused on the development and refinement of analytical and numerical models of trains and train-structure interaction, the improvement of the numerical algorithms for the efficient solution of the equations of motion of the train subsystem, and the methods for coupling the structure and the train during the simulation (Tanabe *et al.*, 2008; Zhai *et al.*, 2019; Zeng, Liu and Wang, 2022). These recent developments are useful for the evaluation of specific sections of bridges under defined running conditions and earthquake scenarios, but they become too costly when multiple scenarios and/or infrastructures are needed to be modeled, e.g., for risk analyses of the system at the network level. Nowadays, plenty of attention is being placed in the evaluation of regional

[1] PhD Student, University of California Berkeley, Berkeley, United States, miguel.gomez.f@berkeley.edu
[2] Associate Professor, University of California Berkeley, Berkeley, United States

resilience of infrastructure, including housing units, tall buildings, and transportation networks, but tools to predict regional resilience of railway systems are needed as well. An accurate but computationally efficient model capable of capturing the global response of the train-structure system would provide a useful tool for researchers to use when performing a regional risk analysis of railway infrastructure and, at the same time, shed light on the main parameters that control the response of the coupled train-structure system. In this paper, a simplified model for the analysis of coupled train-structure interaction is proposed and used to evaluate the running safety in a case study involving the railway network of the San Francisco Bay Area, trying to address the following questions:

- Does the nonlinear behavior of the structure influence the running safety of the train under seismic loading?
- Is a decoupled train-structure model sufficiently accurate to capture the response of the structure and the train?
- Does overturning limit the lateral force the train transmits to the structure?

To answer these questions, a simplified analytical model is proposed in three components: a vehicle model, a structure model, and a rail-wheel interaction model. Each portion of the model is then validated separately, and the procedure for the system coupling is described. A suite of ground motions, developed for a specific location in the case study is used to evaluate the running safety of the train for different modelling scenarios, each of which is defined to help answer the questions above.

Description of the Analysis Model

The analysis model presented in this paper can be divided into three components: a vehicle model, a structure model, and an interaction model. In this section, a description of each component of the model is presented, and then, the solution algorithm that allows solving the coupled system is described.

Model of the vehicle

The dynamic behavior of the cars in a train is governed by the properties of the suspension system and the interaction with the ground. A model aimed to accurately describe the behavior of a train must then consider the principal components of the suspension system, and its mechanical properties, in particular its stiffness and damping. Multiple approaches have been proposed in the literature with multiple levels of complexity. In this study, a 2D version of the model used in (Tanabe *et al.*, 2008) is implemented. Three rigid bodies are used to represent the main components of the car and its suspension system, namely the car body, the bogie, and the wheelsets, with 3 degrees of freedom (DOFs) each: lateral displacement, vertical displacement, and rotation about the longitudinal axis, as shown in Figure 1. Linear springs and dashpots oriented vertically and horizontally are used to represent the mechanical components of the suspension system. The equations of motion of the train subsystem can be obtained by making use of D'Alembert's principle of dynamic equilibrium. They are given in matrix form by Equation 1, where M_v, $C_v$and K_v are the vehicle's mass, damping and stiffness matrices respectively, and $P_{ev}(t)$ is the vector of external forces acting on the vehicle components, including the effect of gravity and the contact forces acting on the wheel-rail interfaces. Thus, a total of 9 DOFs are required to define the location of the train subsystem at each time step during the simulation.

$$M_v\ddot{X}_v + C_v\dot{X}_v + K_vX_v = P_{ev}(t) \quad (1)$$

Since the P_{ev} term in Equation 1 includes the contact forces resulting from impacts in the wheel/rail interface, numerical stability is a main concern for the implementation of the model and its solution. Researchers have found that explicit multi-step methods are efficient, and accurate enough for dynamic analysis of TSI. In this paper an explicit method was adopted, first introduced by (Zhai, 1996; Zhai *et al.*, 2019), which was developed as an explicit variation of Newmark's integration algorithm. The method is based on Equations 2 and 3, with ϕ and ψ parameters that can be varied for enhanced performance. For train running safety analyses, the usual selection is $\phi = \psi = 1/2$, and given the common properties of train suspension systems and the contact stiffness, time steps of $\Delta t = 10^{-5}$ are commonly adopted.

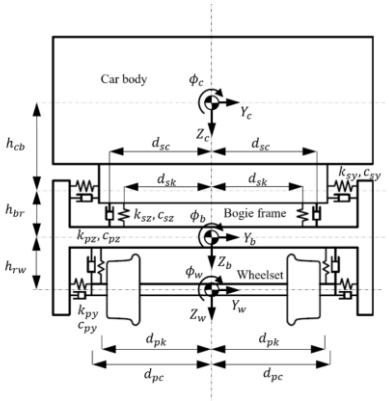

Symbol	Description	Value	Unit
M_c	Mass of car body	29,600	kg
M_t	Mass of bogie	3,621	kg
M_w	Mass of wheelset	648	as
I_{cx}	Mass moment of inertia of car body about X-axis	32,000	kg-m^2
I_{bx}	Mass moment of inertia of bogie about X-axis	944	kg-m^2
I_{wx}	Mass moment of inertia of wheelset about X-axis	362	kg-m^2
H_{cb}	Z distance from car body center of mass (COM) to bogie COM	1.270	m
H_{bt}	Z distance from bogie COM to spring	0.381	m
H_{tw}	Z distance from secondary suspension to wheelset	0.025	m
d_{tk}	Half distance between springs in secondary suspension system	0.545	m
d_{pk}	Half distance between springs in primary suspension system	0.545	m
d_{tc}	Half distance between dashpots in secondary suspension system	0.990	m
d_{pc}	Half distance between dashpots in primary suspension system	0.990	m
K_{sy}	Stiffness coefficient of secondary suspension along Y axis	0.2058	MN/m
K_{sz}	Stiffness coefficient of secondary suspension along Z axis	0.6656	MN/m
K_{py}	Stiffness coefficient of primary suspension along Y axis	0.2058	MN/m
K_{pz}	Stiffness coefficient of primary suspension along Z axis	0.6656	MN/m
C_{sy}	Damping coefficient of secondary suspension along Y axis	17,068	MN/m
C_{sz}	Damping coefficient of secondary suspension along Z axis	17,068	MN/m
C_{py}	Damping coefficient of primary suspension along Y axis	17,068	MN/m
C_{pz}	Damping coefficient of primary suspension along Z axis	17,068	MN/m

Figure 1. Vehicle multi-body dynamics model and definitions. Values in the table correspond to the case study analyzed, described in the following sections.

$$X_v^{(n+1)} = X_v^{(n)} + \dot{X}_v^{(n)}\Delta t + (0.5+\psi)\ddot{X}_v^{(n)}(\Delta t)^2 - \psi\ddot{X}_v^{(n-1)}(\Delta t)^2 \quad (2)$$

$$\dot{X}_v^{(n+1)} = \dot{X}_v^{(n)} + (1+\phi)\ddot{X}_v^{(n)}(\Delta t) - \phi\ddot{X}_v^{(n-1)}(\Delta t)^2 \quad (3)$$

The solution algorithm for the train subsystem involves computing the external forces from the wheel-rail interface model described in the following section, and then integrating the vehicle's equations of motion by making use of Equations (1), (2) and (3). The contact forces contained in the P_{ev} term are computed using a wheel-rail interface model, which is described next.

Wheel-rail interface model

The train and the structure subsystems are coupled using the contact forces acting in the wheel-rail interface. Although the interface between the wheels and the structure has potentially multiple additional components (Zhai *et al.*, 2019; Zeng, Liu and Wang, 2022), the derailment and the train behavior is mostly controlled by this contact interface and its geometry. To accurately describe the behavior of the wheels running on the tracks the model needs to be capable of describing three running regimes: full contact, loss of contact in one wheel, and full detachment.

In this paper, a grid method is implemented to track the coordinates of the points of contact in the wheel-rail interface. The inputs to the model are the geometries of the wheel and rail profiles, along with the location and rotations of the wheelset and the rails. A fine discretization, needed to track the contact points with sufficient accuracy, is implemented using piecewise Hermite polynomials, and then a linear transformation is used to bring the rail and wheel profile descriptions to the track coordinate system. Relevant definitions are provided in Figure 2. The contact is identified by computing the vertical distance, in track coordinate system, between the points corresponding to the wheel and the rail at a specific time; this is expressed by Equation 4, where $z_{R,tr}$ represents the vertical coordinate of the grid points of the rail in track coordinate system, and $z_{W,tr}$ represents the vertical position of the grid points of the wheel in track coordinates.

$$\delta_z = z_{R,tr} - z_{W,tr} \quad (4)$$

When δ_z is positive or zero, no contact is identified; if δ_z takes on negative values, then there is contact at that point. Since this evaluation is done for all the points in the grid, this simple calculation allows to detect multiple contact points at once. In fact, for most cases, not only one node in the grid will result in a negative value (i.e., contact), but many of them will generate a contact area/patch. Since it is convenient to define a single location for applying the total contact force and avoid integrating stresses, the point of maximum absolute indentation δ_{max}, as defined in Figure 2 is used. The indentation is defined as the maximum normal displacement in the grid and will be used later to compute the normal contact force. In addition to the indentation, the angle of the plane of contact can also be calculated, which gives the direction of the normal and tangential forces to be used to compute P_{ev}.

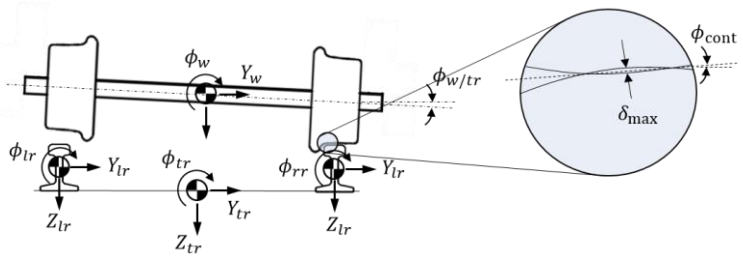

Figure 2. Definition of coordinate systems and indentation for contact evaluation

The normal force resulting from the wheel-rail interface interaction is computed using a modified version of the Hertz theory, introduced by Hunt and Crossley, which includes energy dissipation after impacts. A review on such theories can be found in (Rodrigues da Silva *et al.*, 2022). Equation 5 describes the model, where δ is the indentation between the surfaces in contact, $\dot{\delta}$ is the temporal rate of change of the indentation, K is a stiffness parameter that depends on the material properties and the geometry of the surfaces in contact, and χ is the so-called hysteretic parameter, which incorporates damping to the contact when an impact occurs and depends on the coefficient of restitution.

$$N = \left(K + \chi\dot{\delta}\right)\delta^{\frac{3}{2}} \tag{5}$$

The stiffness parameter K is defined by Equation 6, where E_s is the Young's modulus of the materials (both are assumed equal), r is the radius of curvature at the point of contact, and A and B are the curvatures of the surfaces in contact. The hysteretic parameter χ is defined by Equation 7, with c_r the coefficient of restitution of the bodies in contact.

$$K = \frac{4E_s}{3}\sqrt{\frac{1}{r^3}\frac{1}{A+B}} \tag{6}$$

$$\chi = \frac{3K(1-c_r)}{2\dot{\delta}} \tag{7}$$

In addition to the normal forces, tangential forces also develop in the contact interface. For running safety analyses, these forces are usually calculated using Kalker's linear theory, in which the tangential forces are proportional to the creep occurring in the contact interface, as defined by the following Equations (Kalker, 1990).

$$\begin{aligned} F_x &= -f_{11}\xi_x \\ F_y &= -f_{22}\xi_y - f_{23}\xi_{sp} \\ \xi_x &= \frac{V_{w1} - V_{r1}}{V} \\ \xi_y &= \frac{V_{2w} - V_{r2}}{V} \end{aligned} \tag{8}$$

In Equations (8) F_x and F_y are the tangential forces in the longitudinal and transverse directions, respectively; ξ_x and ξ_y are the creep in the longitudinal and transverse directions; $V_{w1} - V_{r1}$ is the relative velocity between the wheel and the rail in the longitudinal direction; $V_{w2} - V_{r2}$ is the relative velocity between the wheel and the rail in the transverse direction, and V is the running speed of the train.

Model of Structure

Typical elevated structures for railway systems consists of long bridges with multiple piers, each with one or more columns. The model presented here assumes that each pier consists of a single column, whose nonlinear behavior is concentrated at the bottom, near the foundation, in the form of a plastic hinge. The model is a 3DOF cantilever column, as shown in Figure 3, with two DOFs representing the lateral translation and rotation at the top of the column, and one additional DOF at the base to allow inserting a rotational nonlinear spring that represents the plastic hinge. The equations of motion of the structure, subjected to a horizontal ground shaking $\ddot{u}_g$, can be written as:

$$M_s\ddot{X}_s + C_s\dot{X}_s + F_{rs} = -M_s\iota\ddot{u}_g \tag{9}$$

Where M_s and C_s are the mass and damping matrices of the structure, F_{rs} is the vector of resisting forces, which for a linear-elastic analysis are simply K_sX_s, with K_s the stiffness matrix of the structure. X_s contains all three DOFs of the structure $X_s = [u, \theta_1, \theta_2]^T$, as defined in Figure 3. The mass matrix can be easily assembled as a diagonal matrix with entries equal to the translational (m_s) and rotational (I_θ) mass moments of inertia of the corresponding DOFs. The tangent stiffness matrix can also be defined based on the elastic properties of the beam element (E_s,L_c,I_s), and the tangent stiffness of the nonlinear spring included at the base $k_{t\theta}$. The model for the nonlinear spring is based on a Bouc-Wen type of material, which is described later in this section. The Rayleigh damping formulation is used to define the damping matrix C_s for a damping ratio of $\zeta = 0.02$.

$$K_t = \frac{E_sI_s}{L_c^3}\begin{pmatrix} 12 & 6L_c & 6L_c \\ 6L_c & 4L_c^2 + k_{t\theta}\left(\frac{L_c^3}{E_sI_s}\right) & 2L_c^2 \\ 6L_c & 2L_c^2 & 4L_c^2 \end{pmatrix} \tag{10}$$

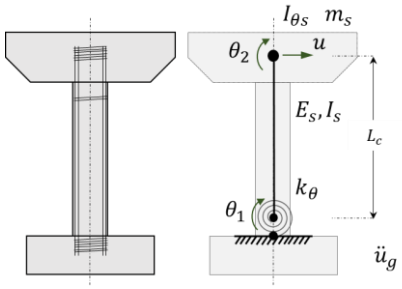

Figure 3. Three-DOF bridge pier model (beam with plastic hinge)

The plastic hinge behavior is modeled using a Degraded Bouc-Wen Model (DBWM), specifically the one presented in Pelliciari *et al.* (2020), formulated for reinforced concrete elements, and that features pinching and stiffness and stress degradation. By this model, the resisting moment of the plastic hinge is a function of the rotation $\theta_1(t)$ and the hysteretic parameter $z(t)$:

$$M_\theta(\theta_1(t), z(t), t) = \alpha k_p(\epsilon)\theta_1(t) + (1-\alpha)k_p(\epsilon)z(t) \tag{11}$$

with:

$$\dot{z} = A(d_i)\dot{\theta} - \beta(d_i)\left(\left|\dot{\theta}\right||z|^{n-1} + \eta_0\dot{\theta}|z|^n\right) \tag{12}$$

In the previous equations, α is the ratio between the final tangent stiffness and the initial elastic stiffness, k_p is a degraded stiffness, whose value depends on the normalized hysteretic energy ϵ, which corresponds to the energy dissipated by the plastic hinge, normalized by the mass of the structure. The model recognizes the effect of the number of cycles and the magnitude of the largest cycle in the degradation of strength and stiffness for RC elements by means of a Damage Index d_i, which is used to represent the strength and stiffness degradation during the simulation. More details on this model are presented in Pelliciari *et al.* (2020).

Coupling algorithm

All the components previously defined are merged into a single simulation workflow, which is described in detail in Figure 4. In summary, the computation is first set up by creating the mass, stiffness and damping matrices of the structure and the train separately. Based on the initial conditions, specifically the initial displacements, the contact forces are computed and then applied to the structure in a first time-step. These forces, and the effective forces generated by the ground motion, are applied to the structure, and one structure time-step is computed using the nonlinear Newmark's method to get the new structural displacements. With the updated structural DOFs, the updated track location is evaluated, and then used to recompute the contact forces, which are then applied to the train subsystem, solving the equations of motion of the train for the updated set of external forces P_{ev} with Zhai's (Zhai, 1996) explicit algorithm.

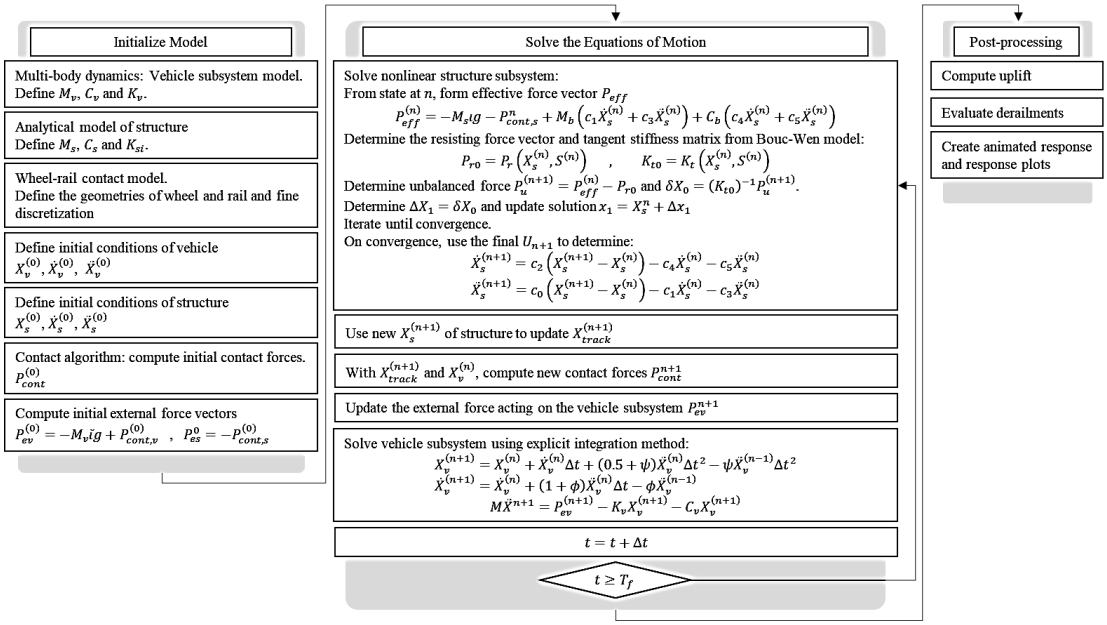

Figure 4. Solution algorithm for the coupled system

Running Safety Assessment Methodology

The model is used to analyze the running safety of trains on a section of the Bay Area Rapid Transit (BART) railway system. A more detailed description of the case study is presented later in this section. The steps to perform the running safety analysis are listed below:

1. First, the case study was set up, and the train and structure models developed are validated against reference values.
2. A suite of 20 ground motions are selected to match 4 different hazard levels at the site of the case study: 50%, 10% and 2% probability of exceedance (PoE) in 50 years, as defined per ASCE 7-16 (ASCE/SEI, 2017b) as serviceability earthquake (SE), design earthquake (DE) and maximum considered earthquake (MCE) levels respectively, and the basic safety earthquake level defined in ASCE 41-17 (ASCE/SEI, 2017a) with a 5% probability of exceedance in 50 years.
3. A set of fully coupled analyses was performed with the proposed model under the assumption of linear-elastic behavior of the structure, using the ground motions defined in (2) for all 4 hazard levels. A similar set of analyses was performed considering nonlinear behavior in the structure, activating the plastic hinge at the base of the column.
4. Two sets of decoupled analyses were performed with the proposed model, one with linear elastic structural behavior, and the second with nonlinear behavior of the column.
5. A final set of at-grade simulations was performed. These simulations consist of applying the ground motions directly at the rail level, not considering the structure in the simulation at all.

Description of the case study

In operation since the 70's, the Bay Area Rapid Transit is an interurban heavy-rail public transit system serving the San Francisco Bay Area, in California. From the total 131 miles of tracks, approximately 25% runs over elevated structures, and the remaining 75% runs either underground or at grade. BART cars are wider than the usual trains that run in Europe or in other locations in the US. The standard gauge (inner rail-to-rail distance) worldwide is 1,435 mm, while the BART track gauge is 1,676 mm, which results in wider cars, and therefore, improved lateral stability. A picture of a typical modern BART car is shown in Figure 5, along with a diagram with general dimensions.

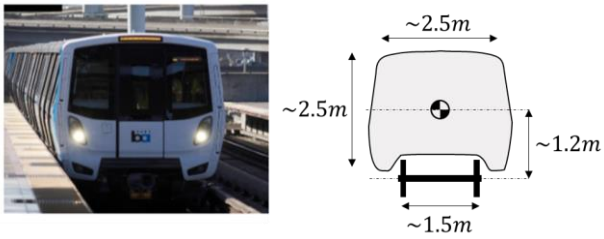

Figure 5. Left: picture of a modern BART train. Right: general dimensions of a BART car.

The selected location of present case-study is an elevated railway near Berkeley, California. The elevated structure was built in the 1960's and consists of 63 RC single-column piers. The columns are octagonal in section shape, and their mean height is 60 ft above ground. A stiff beam at the top of each column provides enough space for two tracks, each placed on top of post-tensioned concrete beams simply supported over the piers. According to as-built information, the piers were constructed with a longitudinal reinforcement ratio of $\rho_l \approx 2\%$, and a transverse reinforcement ratio of $\rho_v \approx 0.7\%$. With an aspect ratio of H/D = 4.8, the columns in this section of the BART system are expected to be slender enough so their inelastic behavior is controlled by the formation of a flexural plastic hinge at the base.

The present case study is used to test the model and evaluate the running safety of BART trains in the section using the proposed model.

Results and Discussion

Characteristics of the vehicle model

To evaluate the pertinence of the parameters used in the train model, an eigenvalue analysis is performed on the vehicle system, fixing the degrees of freedom corresponding to the wheelset. 6 modes of vibration could be identified, 3 of which are comparable to reference values, provided by BART, and by a detailed FEM model of the BART car. Table 1 shows that the values obtained by the proposed model are comparable to those obtained by the more complex FEM model, and they are also consistent to the ones provided by BART. The 3 principal modal shapes are shown in Figure 6.

Mode #	Mode of vibration	This study	BART ref.	FEM model
1	Carbody Lower Sway	0.29	0.31	0.33
2	Carbody Upper Sway	1.01	0.96	0.59
3	Carbody Bounce	1.03	1.28	1.07

Table 1. Results of eigenvalue analysis and comparison with reference values.

Definition of the structure model

The model is built and calibrated against an OpenSees finite element model (FEM). The FEM model was built with available as built information and adopting fiber sections with nonlinear concrete and rebar materials. The FEM model was subjected to multiple cycles of displacements to obtain the force-deformation loops, which were compared against experimental tests to confirm that the shape of the hysteresis loop was consistent with the real behavior of columns with the defined properties of reinforcement ratios (longitudinal and transverse), axial load ratio, shape factor, and material strengths. The experimental database is part of the DEEDS database system (DEEDS, 2023).

The parameters of the degraded Bouc-Wen model were selected to match the cyclic response of the FEM model when subjected to the same prescribed displacements. A set of ground motions were used to further validate the behavior of the DBWM under dynamic loading. Figure 6 shows the resulting cyclic response of the FEM model and the proposed model with DBWM, and the compared response histories when subjected to ground shaking. The model is able to capture the shape of the hysteresis loops of the FEM model and provides a good approximation to the displacement time history for the ground motion.

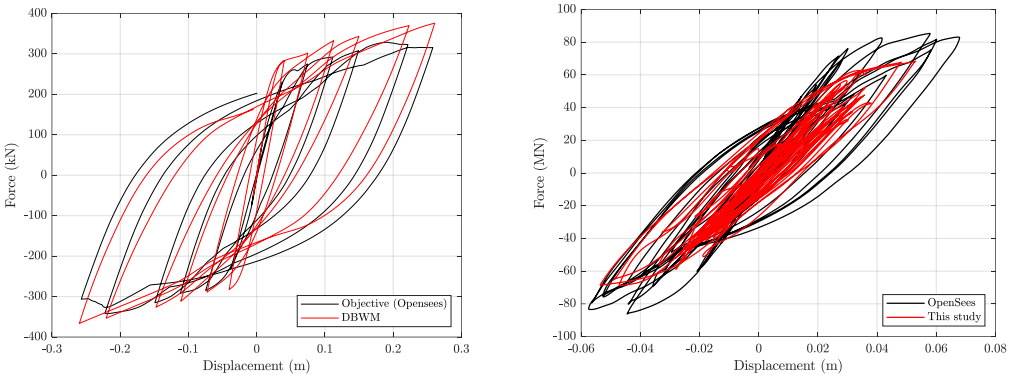

Figure 6. Comparison of OpenSees and DBWM.

Running safety assessment

The running safety assessment is done in terms of how close to the derailment condition the train comes when the system is subjected to ground shaking. Since for all cases analyzed the derailments were observed to happen in a slide-off mode, the derailment condition can be defined as the wheelset-track relative rotation needed to begin the slide-off mode. Once this condition is achieved, the likelihood of derailment is very high, since the derailment mechanism has already started. The peak rotational uplift is then defined as the peak relative rotation between the wheelset and the tracks, and this value is normalized to the rotation required for the uplift onset, as defined previously. The results are shown in Figure 7, where the normalized uplift is plotted as a function of the peak bridge velocity (PBV), and the peak bridge acceleration (PBA). Since the train runs on the tracks, which lie on the bridge, the response of the train does not depend as much on the ground motion characteristics (PGDV or PGA) as it does on the structural displacements, velocities and accelerations. In particular, PBV was found to be well correlated with the onset of uplift, and therefore, with the likelihood of derailment. The reason behind this phenomenon is the fact that a single acceleration spike does not generate derailment, but a consistent acceleration in one direction is needed to reach the point where the system derails. In consequence, the velocity at the bridge level is expected to be well correlated with uplift and derailment as shown in Figure 7. Figure 7 also includes information on the effect of using a nonlinear or a linear model for the structure. Generally speaking, a nonlinear model for the bridge provides smaller uplift values, since the PBVs are lower, due to increased damping. However, in some cases, the frequency content of the ground motion, and the resonant frequencies of the structure and the train, might generate a situation where there is an amplification of the bridge response after damage (period lengthening), increasing the uplift values and the derailment likelihood.

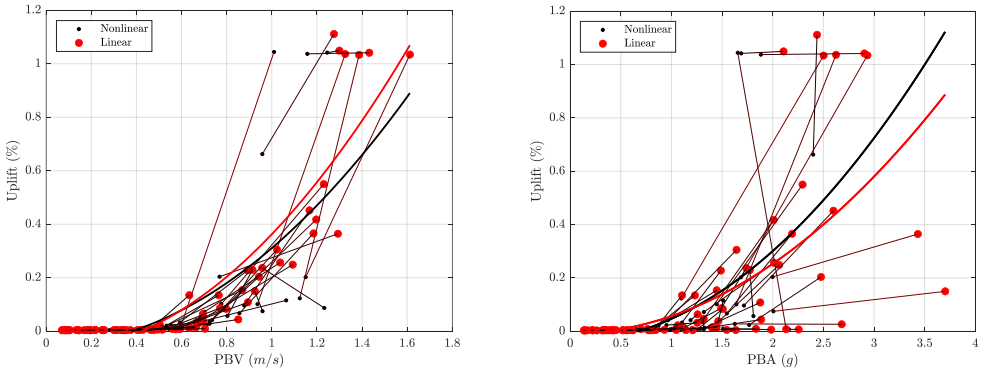

Figure 7. Observed rotational uplift as a fraction of the onset of derailment

Comparison between coupled and decoupled analyses

A common assumption when studying the running safety of trains is assuming that a decoupled analysis is enough to capture the dynamic response of both train and structure. For this type of analysis, the structure is first subjected to a ground shaking, which allows computing the response

of the structure, and then the obtained displacements are used to analyze the response of the train separately. 480 decoupled analyses were evaluated, which were compared to the results of the coupled analyses done in the previous section. We can compare the structural response for both modeling assumptions, specifically in terms of peak displacements and peak accelerations. Figure 8a shows a comparison of the peak lateral displacements at the top of the structure for coupled and decoupled analyses. If the model is linear elastic, the responses for the decoupled model were found to be about 10% larger, in mean, than the displacements of the coupled models. This is due to a combination of additional damping in the contact interface, since for a decoupled model the relative displacements in the contact interface are expected to be larger (i.e., the sliding regime is predominant during the simulation), and larger impacts happening out-of-phase with respect to the structural response, which further reduces the response of the structure in terms of displacements. For nonlinear models, the differences tend to disappear, since the nonlinear model is able to dissipate the large energy caused by the instantaneous impacts in the decoupled model. In terms of accelerations, the same behavior is observed, with larger values observed in the decoupled cases. The differences, however, are smaller than for the displacements.

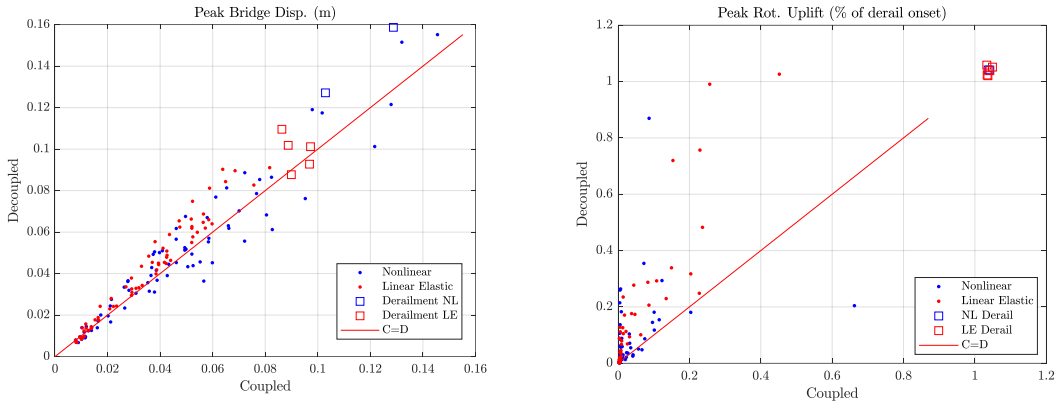

(a) (b)

Figure 8. Comparison of structure and train response for coupled and decoupled analyses

A large difference was obtained in the peak rotations at the top of the column for nonlinear and linear analyses. Although in terms of structural response, the excess rotation does not generate a big difference, this does influence the train response: more derailments and larger uplift values are obtained for decoupled linear elastic analyses, as shown in Figure 8b.

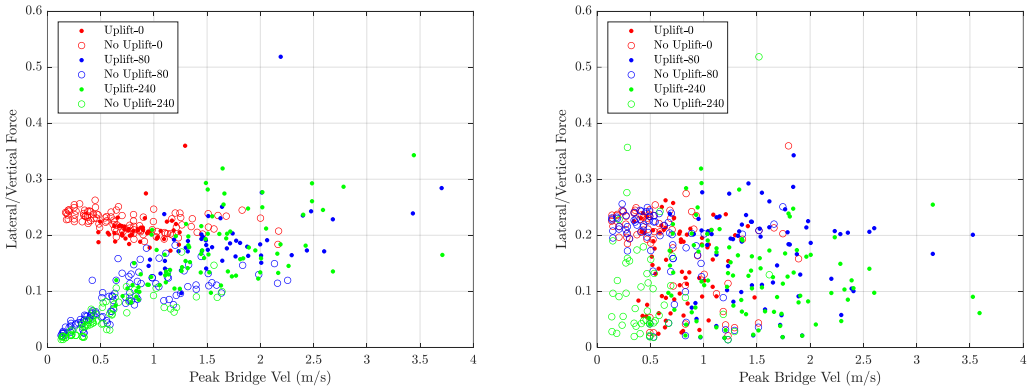

Figure 9. Comparison of structural response for coupled and decoupled analyses

Lateral forces in the train

For the coupled analyses, the lateral forces are capped at a value that is slightly higher than the friction force, due to the curvature of the rails/wheel surface. Short-duration impact forces are not considered in the plots of maximum lateral force shown in Figure 10, since they do not govern train derailment structural damage. For the decoupled analyses, however, the lateral force cap is not as clear as for the coupled analyses, with much higher scatter in the data. The fact that the

response becomes more unpredictable is not a surprise, since the interface in the decoupled model is expected to have larger relative displacements, and therefore, the impacts play a larger role in the response.

Conclusions

A simplified analytical model is presented to perform running safety analysis of trains running on elevated structures. The model is based on commonly used theories of train-structure interaction but simplified with two main assumptions: only the transverse behavior is considered for evaluation of derailment, thus only a 2D model is adopted; and the train-structure interface consists of only the wheel-rail contact interaction. The proposed model is capable of capturing the nonlinear behavior of the structure, as well as the dynamic properties of bridge and train. It can provide an estimate of the likelihood of derailment under seismic conditions.

In terms of the running safety analysis performed, the train response was quantified with respect to the structural vibration. The Peak Bridge Velocity (PBV) was found to be well correlated with the amount of uplift and the derailment likelihood; therefore, fragility curves for derailment of trains could be developed in the future using this response parameter. Using a decoupled analysis for the analysis of the running safety of trains was found to provide a good estimate of the coupled response and tended to be conservative. Future research will include regional simulations using the proposed model to assess the derailment likelihood at a network level for the BART system.

References

ASCE/SEI (2017a) *ASCE/SEI 41-17, Seismic Evaluation and Retrofit of Existing Buildings*, *Seismic Evaluation and Retrofit of Existing Buildings*.

ASCE/SEI (2017b) *ASCE 7-16: Minimum Design Loads and Associated Criteria for Buildings and Other Structures*. American Society of Civil Engineers.

DEEDS (2023) 'NEES Database: Structural Performance for Spiral Concrete Columns'. Available at: https://datacenterhub.org/dataviewer/view/neesdatabases:db/structural_performance_database_for_spiral_concrete_columns/.

Federal Railroad Administration (2023) *Freight Rail Overview*. Available at: https://railroads.dot.gov/rail-network-development/freight-rail-overview.

Kalker, J. (1990) *Elastic Bodies in Rolling Contact Three-Dimensional*.

Pelliciari, M. *et al.* (2020) 'A degrading Bouc–Wen model for the hysteresis of reinforced concrete structural elements', *Structure and Infrastructure Engineering*. Taylor & Francis, 16(7), pp. 917–930. doi: 10.1080/15732479.2019.1674893.

Rodrigues da Silva, M. *et al.* (2022) 'A compendium of contact force models inspired by Hunt and Crossley's cornerstone work', *Mechanism and Machine Theory*. Elsevier Ltd, 167(July 2021), p. 104501. doi: 10.1016/j.mechmachtheory.2021.104501.

Tanabe, M. *et al.* (2008) 'A simple and efficient numerical method for dynamic interaction analysis of a high-speed train and railway structure during an earthquake', *Journal of Computational and Nonlinear Dynamics*, 3(4), pp. 1–8. doi: 10.1115/1.2960482.

The Japan Times (2022) *How Japan's bullet trains keep passengers safe during an earthquake*. Available at: https://www.japantimes.co.jp/news/2022/03/18/national/tohoku-train-derailment-shinkansen/.

Zeng, Z. P., Liu, F. S. and Wang, W. D. (2022) 'Three-dimensional train–track–bridge coupled dynamics model based on the explicit finite element method', *Soil Dynamics and Earthquake Engineering*. Elsevier Ltd, 153. doi: 10.1016/J.SOILDYN.2021.107066.

Zhai, W. *et al.* (2019) 'Train–track–bridge dynamic interaction: a state-of-the-art review', *Vehicle System Dynamics*, 57(7), pp. 984–1027. doi: 10.1080/00423114.2019.1605085.

Zhai, W. M. (1996) 'Two simple fast integration methods for large-scale dynamic problems in engineering', *International Journal for Numerical Methods in Engineering*, 39(24), pp. 4199–4214. doi: 10.1002/(SICI)1097-0207.